Photocatalytic activity of Fe/Ti-based compounds obtained from ferro-titaniferous mineral sands via a simple soft chemistry route

Salomé Galeas, Carla S Valdivieso-Ramírez, Patricia I Pontón, Vincent Goetz, Victor H Guerrero

Photocatalytic activity of Fe/Ti-based compounds obtained from ferro-titaniferous mineral sands via a simple soft chemistry route

Photocatalytic activity of Fe/Ti-based compounds obtained from ferro-titaniferous mineral sands via a simple soft chemistry route

Salomé Galeas[1,2], Carla S. Valdivieso-Ramírez[1], Patricia I. Pontón[1], Vincent Goetz[3] and Victor H. Guerrero[1,*]

[1] Department of Materials, Escuela Politécnica Nacional, Quito 170525, Ecuador
[2] University of Perpignan Via Domitia, 52 Paul Alduy, 66100 Perpignan, France
[3] PROMES CNRS, UPR 8521, Rambla de la Thermodynamique, 66100 Perpignan, France

[*]Corresponding author: victor.guerrero@epn.edu.ec

Abstract. Fe/Ti-based compounds were synthesized from ferro-titaniferous mineral sands using aqueous oxalic acid under subcritical water (sCW) conditions (135°C/50 bar/4 h) and their photocatalytic activity was evaluated against methylene blue or caffeine under UV-A and visible radiation. The X-ray diffraction and Raman spectroscopy analyses revealed that the as-synthetized compounds were mainly comprised of ferrous oxalate, followed by titanium dioxide. This proved the complete transformation of the mineral precursor within 4 h using oxalic acid/sCW as the reaction medium. The photocatalytic studies showed that methylene blue and caffeine were photodegraded under UV-A and visible radiation by the as-synthesized Fe/Ti-based compounds. Methylene blue removal was up to 92.8 and 97.4% after 6 hours under UV-A or visible irradiation, respectively. Caffeine removal, however, reached 69.3 and 59.6% after 16 h of exposure to UV-A and visible light, respectively. The as-synthesized compounds can be potentially used as a ferrous-based catalyst in heterogeneous photocatalysis for decontamination of water systems from organic pollutants.

1. Introduction

Water pollution has become a serious concern worldwide. This pollution is caused by industrial effluents, hospitals and domestic sewage, and threatens water quality and reduces the availability of clean water globally, demanding the development of new materials and technologies for its treatment and decontamination [1]. During the last decades, several processes for removal and degradation of organic pollutants present in water have been widely studied [2–5]. However, conventional treatments as flotation, reverse osmosis, adsorption, ultrafiltration, or biological treatment, are not always efficient and could be energy-consuming [4,6,7].

Advanced oxidation processes (AOPs) have emerged as an alternative for water treatment, as their aim is the complete degradation of organic pollutants into harmless compounds due to the in-situ generation of highly reactive oxygen species (ROS) such as sulfate and hydroxyl radicals [8]. Among these AOPs, photocatalysis is a promising technique, which consists in the generation of hydroxyl radicals by a photocatalytic material under irradiation, leading to degradation of trace organic chemicals [9]. These photocatalytic materials are even more attractive if they can be obtained from widely available and low-cost precursors by using energy efficient and environmentally friendly methods that do not require toxic and expensive solvents [10–13]. Iron-based materials, for example, are widely used in heterogeneous photocatalysis because of their effectiveness, abundance, and low cost [14]. Among iron-based materials, iron oxalate can be obtained by simple reaction of oxalic acid with an iron source, which photocatalytic activity has been reported in literature. In addition, recovery of ferrous oxalate from wastewater streams of washing of heavy metal contaminated soils has been also explored [15] as well as its photocatalytic activity studied on methylene blue (MB) [15]. As such, degradation of MB (20 ppm solution) up to 50 and 90% was reported within 1 and 3 h, respectively, when 0.5 g/L of recovered

ferrous oxalate was used as catalyst under simulated sun light [15]. Also, Hu et al. [16] used ferrous oxalate to degrade MB but in Fenton and photo-Fenton processes. In their case, a combination of 0.5 g/L of catalyst and hydrogen peroxide (30 mg/L) led to 94% and 97.2% of MB (10 ppm solution) degradation within 10 and 15 min, respectively [16]. Hence, the percent degradation was improved under a xenon lamp irradiation (500 W), reaching over 95% within 3 min, and 98.4% in 10 min [16]. The photocatalytic activity of ferrous oxalate has been also explored for degradation of other cationic and anionic dyes like rhodamine B [17] and indigo red [18], respectively. In addition, ferrous oxalate has proven to be effective in the oxidation of the herbicide 2,4-dichlorophenoxyacetic acid [19]. In this context, MB and caffeine were selected as the model pollutants for this study.

MB dye can be used as a suitable pollutant to assess the photocatalytic activity of iron-based photocatalysts and to get an insight on photodegradation of similar chemical compounds that are resistant to biodegradation and are widely present in the large volume effluents of the textile industry that threaten the ecosystem and human health [20]. Likewise, caffeine was selected since it is a common alkaloid, highly soluble in water, extensively found in water bodies, which can negatively impact aquatic life [21]. Currently, studies focused on either MB or caffeine degradation by ferrous oxalate-based catalysts are limited. Therefore, the aim of this work was to first synthesize Fe/Ti-based compounds from ferro-titaniferous mineral sands using aqueous oxalic acid under subcritical water (sCW) conditions (135°C/50 bar/4 h) as an alternative eco-friendly process to conventional mineral acid leaching and further evaluate whether the as-synthetized compounds exert a photocatalytic activity against methylene blue or caffeine under UV-A and visible radiation.

2. Materials and methods

2.1. Materials

Ecuadorian ferro-titaniferous sands from the "El Ostional" beach were used as mineral precursor. Such ferro-titaniferous mineral was reported as an ilmenite hematite solid solution with estimated chemical composition of $0.6FeTiO_3 \cdot 0.4Fe_2O_3$ [22]. Oxalic acid dihydrate was supplied by Merck, caffeine was purchased from Beantown Chemicals and methylene blue from Panreac. All chemicals were analytical grade and used as received. Water from the Milli-Q system (Millipore, Billerica, MA, USA) and N_2 gas (99.9% purity) from Linde (Quito, Ecuador) were used for the subcritical water synthesis.

2.2. Synthesis of the catalysts

The synthesis of the iron-based catalysts from the ferro-titaniferous sands was carried out in a batch stirred high pressure reactor (Berghof BR-500, Germany) following the methodology described by Valdivieso-Ramírez et al. [23], with some modifications. Briefly, 300 g of 1 M oxalic acid solution and 1.75 g of ferro-titaniferous sands were loaded into the reactor. Once the system was assembled and N_2 pressurized, the reaction was set at 135°C, 50 bar and 4 h. The as-synthesized product stream was oven-dried at 60°C for 12 h and stored for characterization and further utilization in the photocatalytic activity test. The sCW synthesis of the catalyst is summarized in Figure 1.

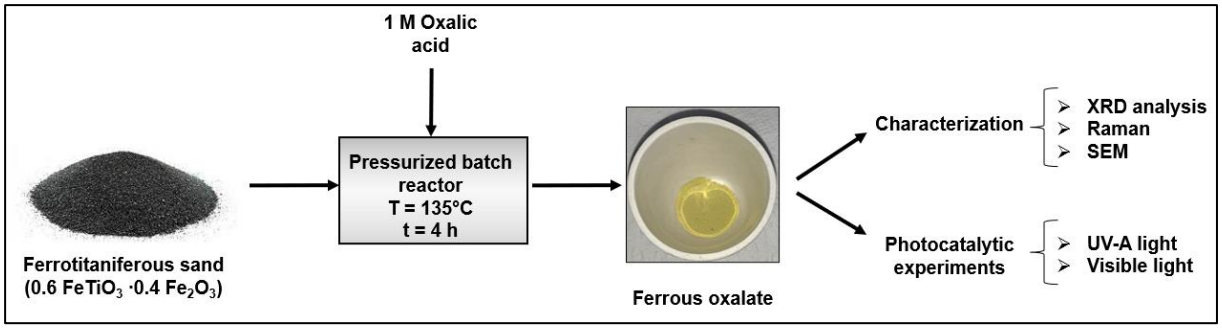

Figure 1. Scheme for the synthesis of iron-based photocatalyst from ferro-titaniferous sands with 1 M oxalic acid at 135° and 50 bar.

2.3. Characterization

X-ray diffraction (XRD) analysis was performed on the as-synthesized product using a Bruker D2 Phaser X-ray diffractometer with CuKα radiation (λ = 1.54184 Å), step size 0.02°, with LYNXEYE XE-T detector (1D-mode). Also, the as-synthesized product was analyzed by Raman spectroscopy using a LabRAM HR Evolution confocal microscopic Raman spectrometer (HORIBA Scientific, France) with a 633 nm laser irradiation set at 12.5 mW of power. Scanning electron microscopy (SEM) images of the as-synthetized product were recorded in a PSEM eXpress (ASPEX, USA) operated in secondary electron mode.

2.4. Photocatalytic activity test

The photocatalytic activity of the as-synthetized iron-based catalyst on methylene and caffeine was evaluated under UV-A and visible radiation according to the method depicted in Figure 2. Such method consisted of an initial dispersion of the aqueous pollutant with the solid catalyst by means of an ultrasonic probe (10 kHz, t=1 min), orbital stirring and subsequent analysis of the filtered solutions by UV/VIS spectrometry (HORIBA, Duetta) at 664 and 272 nm for methylene blue and caffeine, respectively.

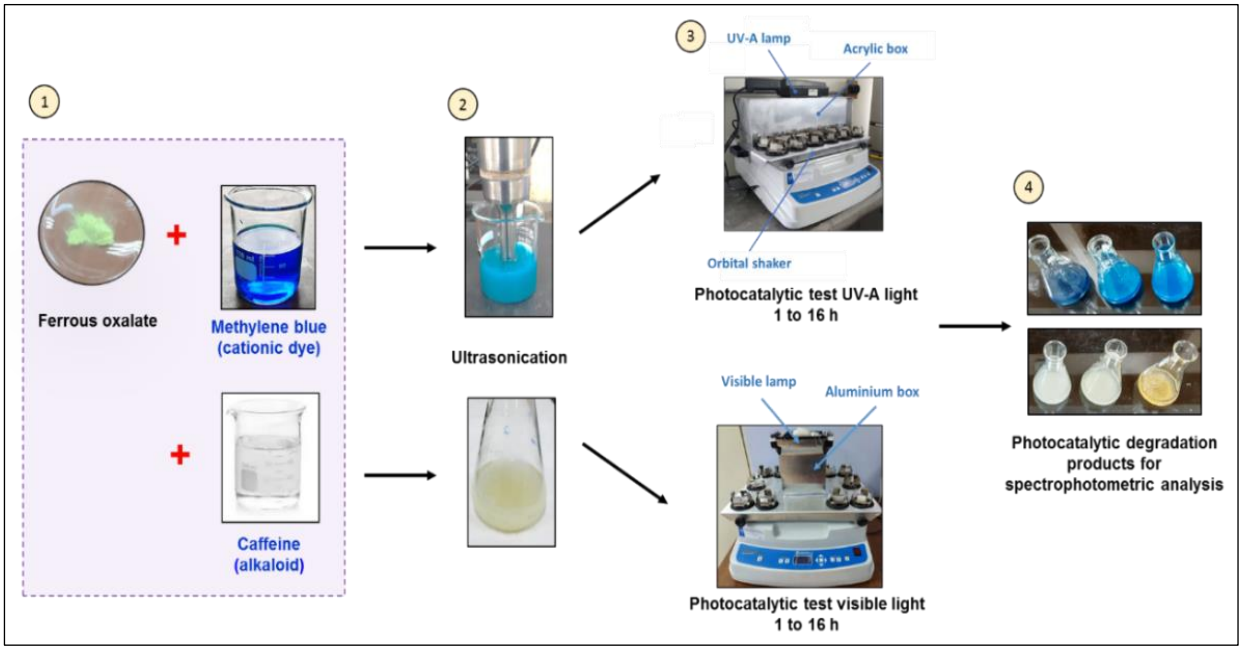

Figure 2. Scheme followed for the photocatalytic tests.

For the photocatalysis test, solutions of methylene blue and caffeine of 10 ppm were used. Also, a working pH of 3.1 was selected based on the reported conditions for Fenton and photocatalytic processes [24]. The catalyst load was 1.5 g/L and the reaction times 1, 3, 6 and 16 h. The photocatalysis was carried out in a chamber equipped with a UV-A or a visible irradiation lamp placed on an orbital shaker set at 150 rpm (TECNAL, model TE-1400). UV-A radiation was supplied by a 6 W UV lamp with light emission at 365 nm (UVP, model UVGL-55), whereas visible light was provided by an 18 W LED lamp (Sylvania, LED panel SQ 18W DL). The experimental conditions used for the photocatalysis of the model pollutants by the as-synthetized iron-based catalyst are detailed in Table 1.

Table 1. Experimental conditions used for the removal of MB and caffeine from aqueous solutions by the as-synthetized iron-based catalyst.

Pollutant	Catalyst	Light source	Reaction times (h)	Experiment
MB 10 ppm	$FeC_2O_4{\cdot}2H_2O$ (135°C-4h) 1.5 g/L	UV-A	1, 3, 6, 16	Photocatalysis
		Visible	1, 3, 6, 16	Photocatalysis
		Darkness	1, 3, 6, 16	Adsorption
	None	UV-A	16	Photolysis
		Visible	16	Photolysis
Caffeine 10 ppm	$FeC_2O_4{\cdot}2H_2O$ (135°C-4h) 1.5 g/L	UV-A	1, 3, 6, 16	Photocatalysis
		Visible	1, 3, 6, 16	Photocatalysis
		Darkness	1, 3, 6, 16	Adsorption
	None	UV-A	16	Photolysis
		Visible	16	Photolysis

3. Results

3.1. Characterization of the as-synthetized catalyst

The X-ray diffractogram of the as-synthesized catalyst is shown in Figure 3. Peaks at diffraction angles (2θ) correspond to ferrous oxalate hydrate $FeC_2O_4{\bullet}2H_2O$ in two crystalline phases, both with the same monoclinic unit cell, but with different values of the lattice parameter (*a*). Peaks observed at 18.7°, 19.1°, 23.1°, 25.0°, 28.3°, 29.9°, 32.5°, 34.0°, 34.5°, 37.7°, 38.4°, 40.8°, 43.2°, 44.7°, 45.1°, 47.3°, 48.3°, 49.5°, 50.4°, 51.2°, and 57.2°, are in accordance with PDF # 23-0293, where $a = 9.84$ Å. The diffraction peaks appearing at 35.5°, 40.1°, 42.8°, 46.0°, 46.8°, 53.1°, 56.4°, and 58.1° correspond to PDF # 72-1305, where $a = 12.06$ Å.

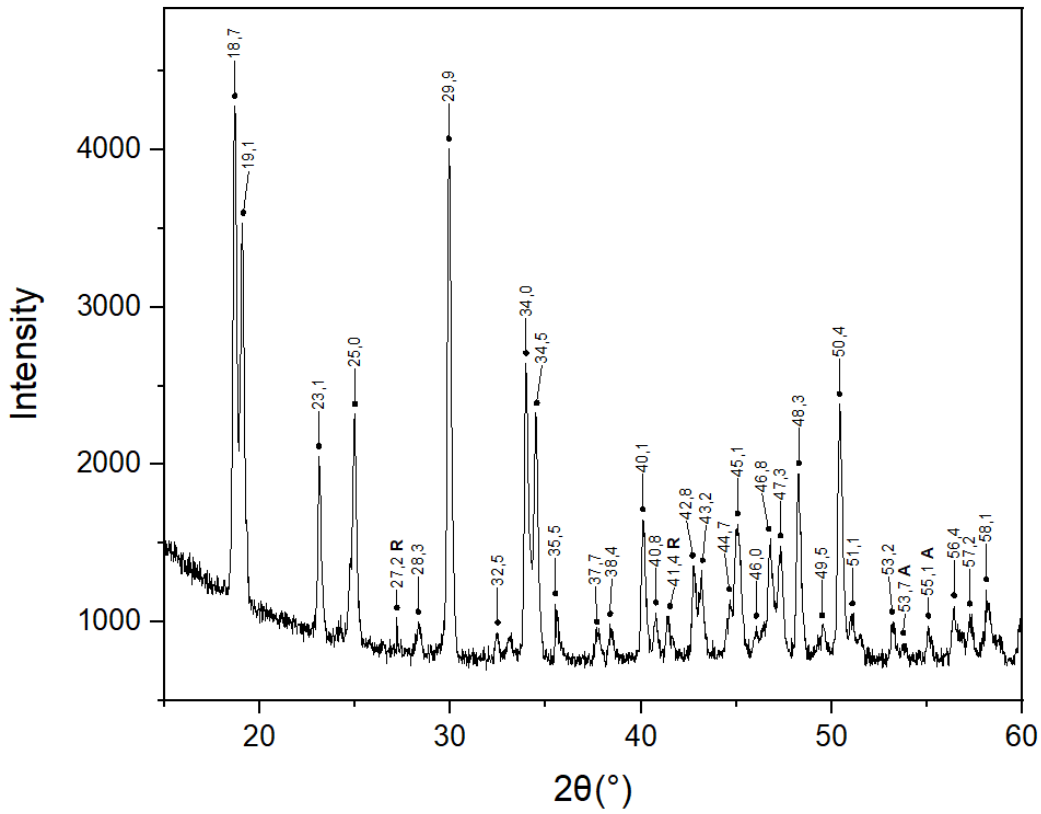

Figure 3. X-ray diffractogram of the as-synthetized product from ferro-titaniferous sands with 1 M oxalic acid at 135°C, 50 bar and 4 h.

The XRD pattern also showed additional peaks which are associated to the presence of titanium dioxide, because Ti is also present in the ferro-titaniferous sand precursor. Diffraction peaks at 2θ values of 27.2° and 41.4°, correspond to rutile phase (PDF 21-1276) and the peaks at 53.7° and 55.1° are ascribed to anatase phase (PDF 21-1272). Since the intensity of these peaks is lower than that of ferrous oxalate, the TiO_2 phases are present in a smaller fraction.

The Raman spectrum of the as-synthetized catalyst, depicted in Figure 4, presents the characteristic bands of ferrous oxalate. The bands observed at 1710 and 1470 cm^{-1} may be assigned to the ν (C=O) stretching mode. Another band at the low wavenumber side of the symmetric stretching mode appeared at 1435 cm^{-1}. The band at 915 cm^{-1} could be attributed to the ν (C–C) stretching mode and the low intensity band at 858 cm^{-1} is assigned to the O-C=O bending mode. The band at 585 cm^{-1} matches with water librational mode and the band at 520 cm^{-1} may be attributed to the symmetric O-C=O bending mode (δ-ring). Bands at 288, 246, and 206 cm^{-1} may be assigned to Fe-O stretching and bending modes [25].

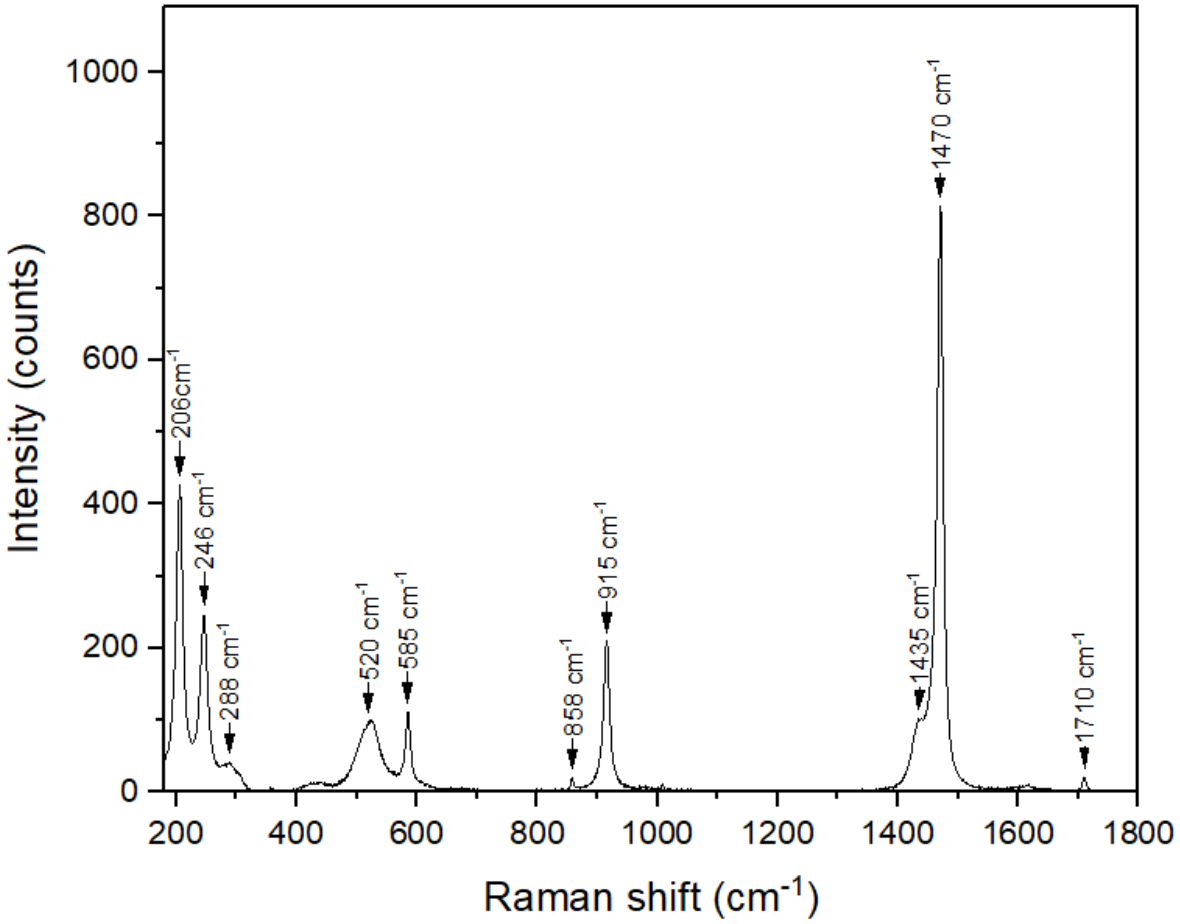

Figure 4. Raman spectra of the as-synthetized product from ferro-titaniferous sands with 1 M oxalic acid at 135°C, 50 bar and 4 h.

In addition, the morphology of the dry as-synthetized product powder was observed by SEM. Figure 5 shows that the as-synthetized product is of heterogenous size and morphology as indicated by the smaller structures with sharp pyramidal shape as well as the presence of submicronic structures with a rhomboidal crystal trend.

The characterization of the as-synthetized product demonstrated that it is mostly composed of ferrous oxalate, which could be potentially used for photocatalysis. Therefore, the photocatalytic activity of the FeC_2O_4-based product was evaluated next.

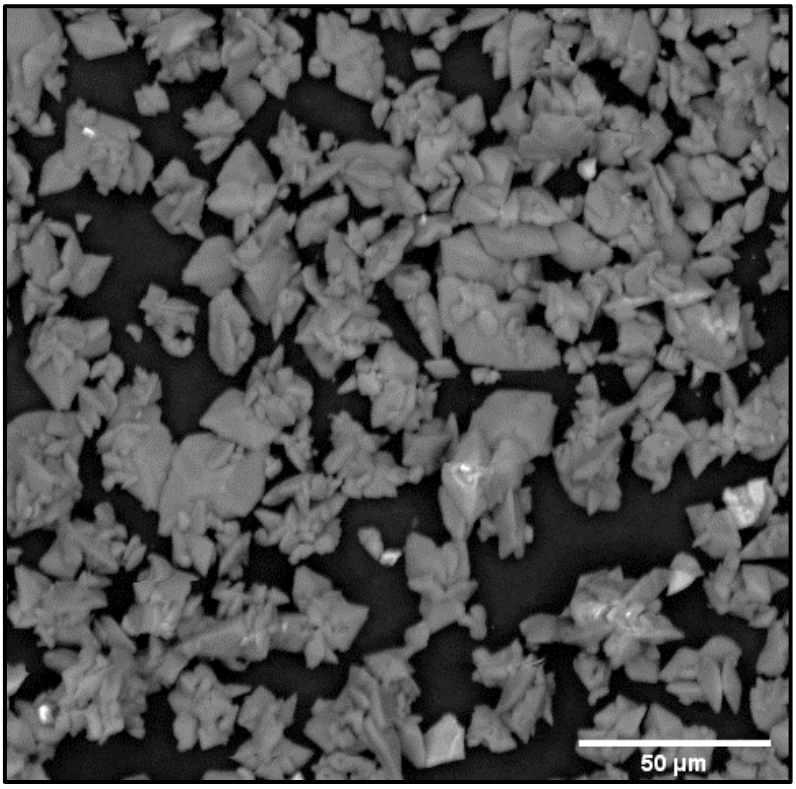

Figure 5. SEM image of the as-synthetized product from ferro-titaniferous sands with 1 M oxalic acid at 135°C, 50 bar and 4 h.

3.2. Photocatalytic activity

3.2.1. Methylene blue removal. Prior to photocatalytic activity tests under UV-A and visible light (Table 1), an adsorption test at 1, 3, 6 and 16 h of contact time was carried out using a methylene blue pristine solution. According to the UV-VIS spectrograph showed in Figure 6, the absorbance of the pristine MB solution got reduced with time, where major removal of MB (27.6%) occurred within 1 h and after 16 h only an additional 2.3 % was removed. However, the highest percent removal was observed at 6 h (37.9%), suggesting that a desorption phenomenon took place within the next 10 h that led to a final percent removal of 29.9%. In addition, no shift of the band of maximum absorption at 664 nm was apparent with time, indicating that adsorption could be the main catalytic mechanism associated with MB removal by the synthesized FeC_2O_4-based catalyst in the absence of external radiation.

Figure 7 shows the UV-VIS spectra of MB photocatalysis by the FeC_2O_4-based synthetized catalyst. According to Figures 7.a and 7.b, photodegradation of MB indeed occurred at either UVA or visible light conditions as an hypsochromic shift from 664 to 628 nm was apparent while the absorbance values got reduced. Interestingly, photooxidation of MB by a TiO_2/UV catalytic system has reported also a hypsochromic shift due to partial consecutive N-demethylation of MB to blue colored compounds such as Azure B, A and C that absorb light at lower wavelengths of 655-648, 634-620 and 612-608 nm, respectively [26]. Although the catalytic system used in this work (FeC_2O_4/UV-light), differs from the one mentioned above, generation of hydroxyl radicals and further oxidation of MB into blue colored analogous compounds can be also expected as FeC_2O_4 has shown to be a highly photosensitive complex that can assist the generation of hydroxyl radicals in the presence of UV-light [27]. As such, the spectra in Figure 7 show a wavelength shift with time from 664 to 628 nm suggesting that the formation of partially demethylated compounds Azure B and Azure A occurred. Nonetheless, further HPLC analysis are recommended for identification and quantification of the above-mentioned compounds.

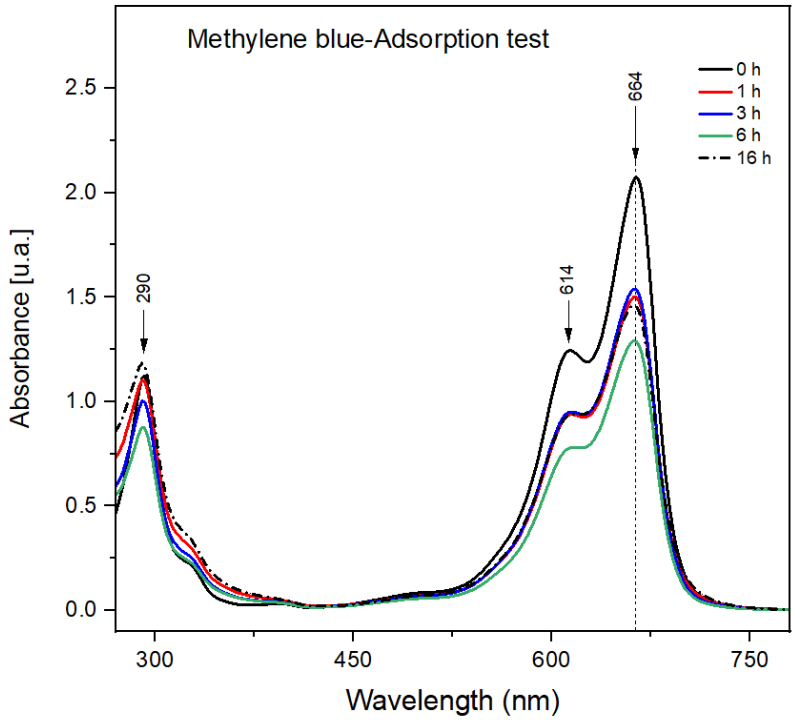

Figure 6. UV-VIS spectra of methylene blue adsorption by the FeC_2O_4-based synthetized catalyst.

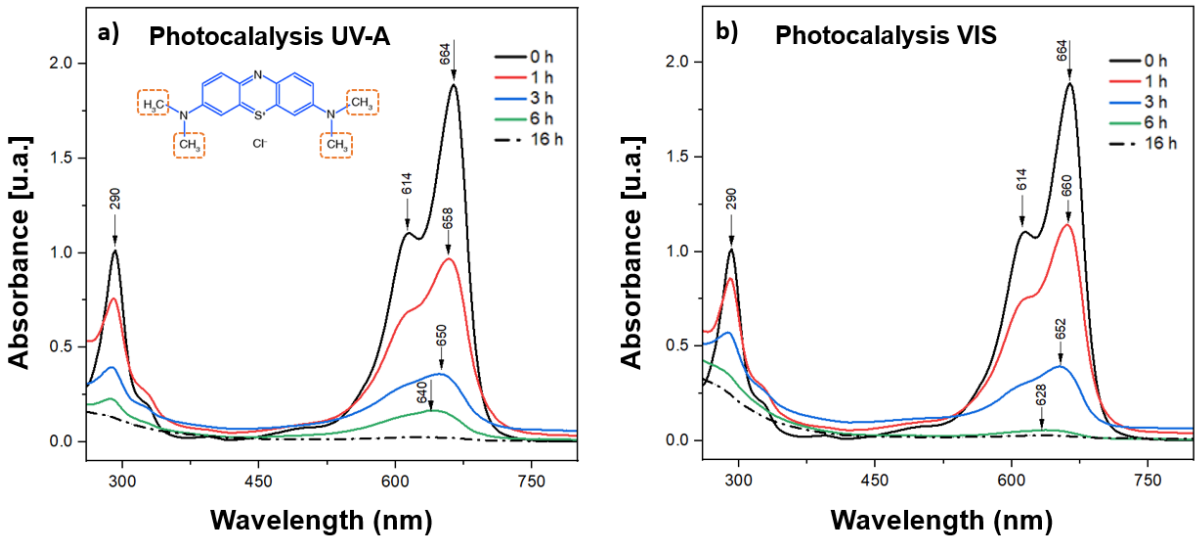

Figure 7. UV-VIS spectra of methylene blue photocatalysis under a) UV-A light and b) visible light by the FeC_2O_4-based synthetized catalyst.

The percent removal of methylene blue under UV-A and visible light radiation is displayed in Figure 8a. According to Figure 8a, the type of radiation source did not influence considerably the removal of methylene blue as the rate of removal was similar for photocatalysis at either UV-A or visible light conditions. As such, percent removal after 6 h reached 93 and 98 % for UV-A and visible light exposure, respectively., and after 16 h, the removal was almost complete. The removal of methylene blue was associated with a gradual change of color intensity, as seen in Figure 8b. In addition, methylene blue removal could be due to adsorption and photodegradation effects as the rate of removal (steepest

slope of the curve removal % vs. time) was the highest within the first hour. Conversely, experiments in the absence of the catalyst were done to determine the stability of pristine methylene blue solution upon exposure to the selected radiation. The percent photolysis was 3.7% for both light sources. Based on the above-mentioned results, the as-synthetized FeC_2O_4-based compound exhibited photocatalytic activity under UV-A and visible irradiation, which is very desirable in photocatalyst to effectively utilize the solar energy.

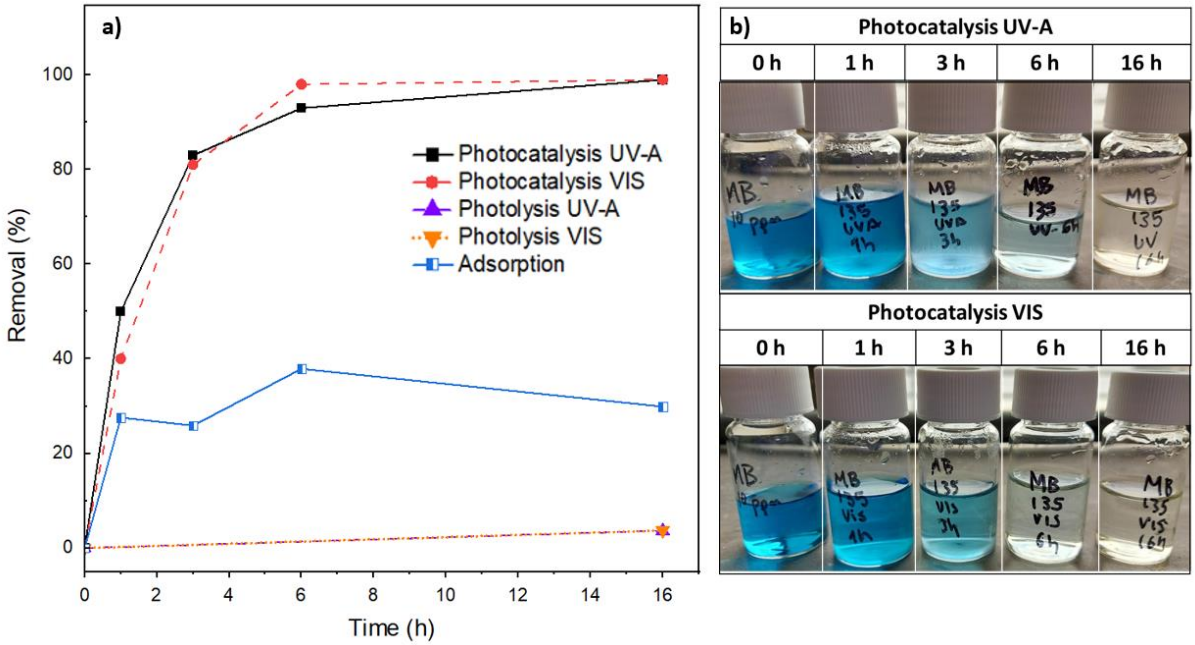

Figure 8. (a) Methylene blue percent removal by absorption, photolysis and photocatalysis via the FeC_2O_4-based synthetized catalyst and b) Methylene blue solutions obtained after photocatalysis under UV-A and visible light irradiation.

3.2.2. Caffeine removal. To evaluate caffeine behavior when in contact with the FeC_2O_4-based synthetized catalyst, an adsorption test at conditions detailed in Table 1 was carried out on caffeine pristine solution. The resulting UV-VIS spectra (Figure 9), showed increased absorbance values with time compared to that of the pristine caffeine solution, suggesting the formation of other compounds possible due to caffeine-iron catalyst interactions. Interestingly, formation of metal-caffeine coordination complexes has been reported for Ca, Mg, Fe, Zn, etc. [28,29]. As such, a binding constant of 59 has been attributed to the Fe^{+2}-caffeine coordination complex [28]. In addition, the absorption of electromagnetic radiation of the iron–caffeine coordination complex has been reported near to the maximum absorption band of pure caffeine at 272 nm [30]. The formation of such coordination complex can resemble to an acid-base reaction where caffeine (Lewis base ligand) donates a pair of electrons to the metal ion Fe^{+2} (Lewis acid) to form the metal-ligand bond [31]. Thus, the iron-caffeine complex can also be considered as a charge-transfer complex, where absorption of radiation is due to an electronic transition from the donor to the corresponding orbital of the acceptor so that the associated molar absorptivity (ε) is high compared to that of molecules that exhibit π, σ and n electron transitions [31]. As such, the increased absorbance values at 272 nm observed in Figure 9 could be associated to the increased light absorption of the newly formed iron-caffeine complex, which molar absorptivity has been reported larger ($>1x10^4$ $M^{-1}cm^{-1}$) than that of pristine caffeine ($>9.74x10^3$ $M^{-1}cm^{-1}$) [32]. Also, as the absorbance is directly proportional to molar absorptivity (ε), the concentration of the absorbing species and the path length (Beer's Law), the increased ε value of the iron-caffeine complex will indeed lead to increased absorbance. Therefore, it can be inferred that caffeine reacts with the iron present in

the FeC_2O_4-based catalyst and forms a soluble iron-caffeine complex, which concentration increases with time.

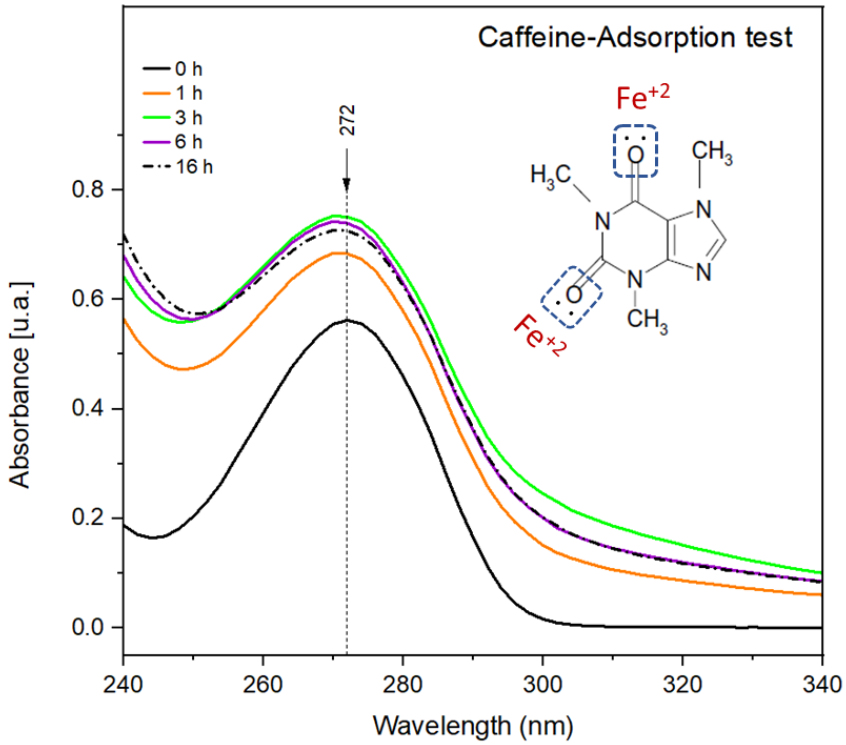

Figure 9. UV-VIS spectra of caffeine adsorption test by the FeC_2O_4-based synthetized catalyst.

Figure 10 shows the UV-VIS spectra of caffeine photocatalysis by the FeC_2O_4-based synthetized catalyst under UV-A or visible light. According to Figures 10.a and 10.b, photodegradation of caffeine indeed occurred as the absorbance values at the maximum absorption wavelength at 272 nm got considerably reduced with time. Also, band broadening was apparent as the time approached to 16 h, possibly due to the formation of intermediate compounds. Demethylation and hydroxylation of caffeine have been reported due to in-situ generation of hydroxyl radicals under Fenton conditions leading to 1,3-dimethyl uric acid and 6-amino-5-(N-formyl methyl amino)-1,3-dimethyl-uracil [33]. Also, the formation of intermediates like 1, 3-dimethyl-2, 4, 5-trioxoimidazolidinetrione and other compounds with mass-to-charge ratio (m/z) of 181.0738, 211.0906 and 227.0834 have been identified by electrospray ionization mass spectrometry (ESI-MS) in the presence of Fe^{+2}/persulfate/UV-light [34], but complete caffeine mineralization (CO_2, H_2O, and NH_3) via the reported photocatalytic systems has to been achieved. As the photocatalytic system used in the present study (FeC_2O_4-TiO_2/UV-A or VIS) resembles to those mentioned above, in the sense of its iron and titanium dioxide content, it could be inferred that the main reactive specie generated during the photocatalysis was the hydroxyl radical; therefore, photooxidation of caffeine could have occurred. In addition, the band broadening exhibited in the UV-VIS spectra obtained from the caffeine solutions after photocatalysis (Figure 10) could be attributed to the presence of intermediates that absorb light at a wide range of wavelengths like the ones similar to uric acid and uracil that exhibit maximum absorption at 290 cm^{-1} [35] and 260 and 300 cm^{-1} [36], respectively.

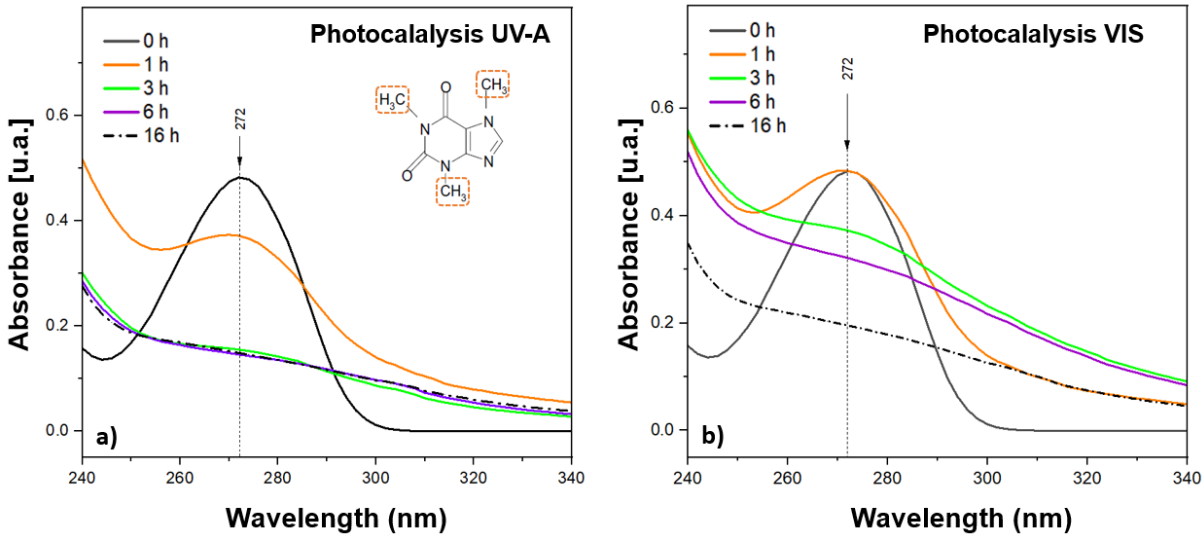

Figure 10. UV-VIS spectra of the solutions after caffeine photocatalysis under a) UV-A light, and b) visible light irradiation by the FeC_2O_4-based synthetized catalyst.

The percent removal of caffeine under UV-A and visible light radiation is displayed in Figure 11. According to Figure 11, the type of radiation source influenced considerably the removal of caffeine as the rate of removal for photocatalysis under UV-A was faster than that of the visible light. As such, percent removal after 6 h reached 70 and 34 % for UV-A and visible light exposure, respectively., and after 16 h, the removal was quite close for both catalytic systems. Nonetheless, the percent photolysis under UV-A was 1.2%, whereas under visible light was negligible. Based on the above-mentioned results, the as-synthetized FeC_2O_4-based compound exhibited photocatalytic activity under UV-A and visible irradiation that led to removal of the alkaloid caffeine.

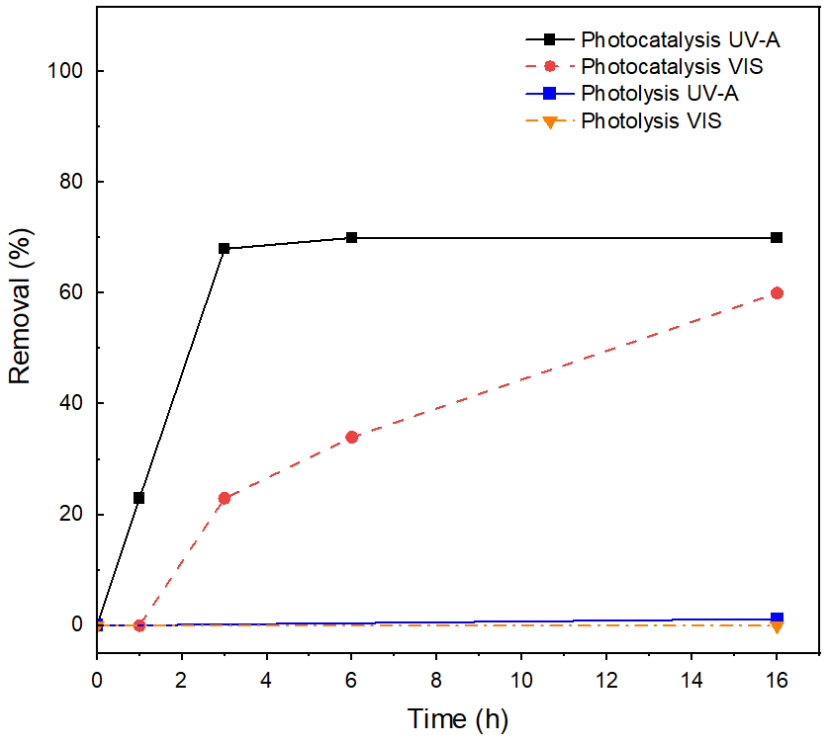

Figure 11. Caffeine percent removal by photolysis and photocatalysis via the FeC_2O_4-based synthetized catalyst

4. Conclusions

The synthesis of Fe/Ti-based compounds from ferro-titaniferous mineral sands using a non-hazardous solvent system (1 M oxalic acid) at subcritical water conditions (135 °C and 4 h) was demonstrated as a feasible alternative to conventional mineral acid leaching. The as-synthetized compound was identified as ferrous oxalate hydrate by XRD. The synthetized ferrous oxalate hydrate exhibited photocatalytic activity under both UV-A and visible light irradiation as methylene blue and caffeine were indeed photodegraded. Therefore, the synthetized ferrous oxalate can be potentially used as a photocatalyst to effectively utilize the solar energy in advanced oxidation processes for wastewater treatment.

Acknowledgements

This research was supported by Escuela Politécnica Nacional (EPN) through the project grant PIJ-18-01. The authors would also like to thank the Electroceramics Laboratory of the Department of Physics (EPN), and the New Materials Laboratory of the Department of Materials (EPN) for material characterization, as well as the FSPI Project - Doctoral Schools, of the French Embassy in Ecuador, financed by the Ministry of Europe and Foreign Affairs.

References

[1] Antonopoulou M, Kosma C, Albanis T and Konstantinou I 2021 An overview of homogeneous and heterogeneous photocatalysis applications for the removal of pharmaceutical compounds from real or synthetic hospital wastewaters under lab or pilot scale *Sci. Total Environ.* **765** 144163

[2] Khan S, Naushad M, Al-Gheethi A and Iqbal J 2021 Engineered nanoparticles for removal of pollutants from wastewater: Current status and future prospects of nanotechnology for remediation strategies *J. Environ. Chem. Eng.* **9** 106160

[3] Mashile G P, Selahle S K, Mpupa A, Nqombolo A and Nomngongo P N 2022 Chapter 8 - Remediation of emerging pollutants through various wastewater treatment processes *Emerging Freshwater Pollutants* ed T Dalu and N T Tavengwa (Elsevier) pp 137–50

[4] Negrete-Bolagay D, Zamora-Ledezma C, Chuya-Sumba C, De Sousa F B, Whitehead D, Alexis F and Guerrero V H 2021 Persistent organic pollutants: The trade-off between potential risks and sustainable remediation methods *J. Environ. Manage.* **300** 113737

[5] Kumar L, Chugh M, Kumar S, Kumar K, Sharma J and Bharadvaja N 2022 Remediation of petrorefinery wastewater contaminants: A review on physicochemical and bioremediation strategies *Process Saf. Environ. Prot.* **159** 362–75

[6] Coha M, Farinelli G, Tiraferri A, Minella M and Vione D 2021 Advanced oxidation processes in the removal of organic substances from produced water: Potential, configurations, and research needs *Chem. Eng. J.* **414** 128668

[7] Xie Z H, Zhou H Y, He C S, Pan Z C, Yao G and Lai B 2021 Synthesis, application and catalytic performance of layered double hydroxide based catalysts in advanced oxidation processes for wastewater decontamination: A review *Chem. Eng. J.* **414** 128713

[8] Ameta R, Chohadia A K, Jain A and Punjabi P B 2018 *Fenton and Photo-Fenton Processes*

[9] Miklos D B, Remy C, Jekel M, Linden K G, Drewes J E and Hübner U 2018 Evaluation of advanced oxidation processes for water and wastewater treatment – A critical review *Water Res.* **139** 118–31

[10] Es-sahbany H, El Yacoubi A, El Hachimi M L, Boulouiz A, Chafik El Idrissi B and El Youbi M S 2022 Low-cost and eco-friendly Moroccan natural clay to remove many bivalent heavy metal ions: Cu2+, Co2+, Pb2+, and Ni2+ *Mater. Today Proc.* 1–7

[11] Ramirez-Muñoz A, Pérez S, Muñoz-Saldaña J, Flórez E and Acelas N 2021 Eco-friendly materials obtained through a simple thermal transformation of water hyacinth (Eichhornia Crassipes) for the removal and immobilization of Cd2+ and Cu2+ from aqueous solutions *Environ. Nanotechnology, Monit. Manag.* **16**

[12] Lessa E F, Nunes M L and Fajardo A R 2018 Chitosan/waste coffee-grounds composite: An

efficient and eco-friendly adsorbent for removal of pharmaceutical contaminants from water *Carbohydr. Polym.* **189** 257–66
[13] Kumar B, Smita K, Galeas S, Guerrero V H, Debut A and Cumbal L 2021 One-Pot Biosynthesis of Maghemite (γ-Fe2O3) Nanoparticles in Aqueous Extract of Ficus carica Fruit and Their Application for Antioxidant and 4-Nitrophenol Reduction *Waste and Biomass Valorization* **12** 3575–87
[14] Rahim Pouran S, Abdul Raman A A and Wan Daud W M A 2014 Review on the application of modified iron oxides as heterogeneous catalysts in Fenton reactions *J. Clean. Prod.* **64** 24–35
[15] Kim S R, Kim S and Kim E J 2020 Photoreaction characteristics of ferrous oxalate recovered from wastewater *Chemosphere* **249** 126201
[16] Hu L, Wang P, Xiong S, Chen S, Yin X, Wang L and Wang H 2019 The attractive efficiency contributed by the in-situ reactivation of ferrous oxalate in heterogeneous Fenton process *Appl. Surf. Sci.* **467**–**468** 185–92
[17] Wang G, Zhou A and Xu Q 2019 α-Ferrous oxalate with different micro scale: Synthesis and catalytic degradation effect to rhodamine B *Solid State Sci.* **91** 54–60
[18] Vedrenne M, Vasquez-Medrano R, Prato-Garcia D, Frontana-Uribe B A, Hernandez-Esparza M and de Andrés J M 2012 A ferrous oxalate mediated photo-Fenton system: Toward an increased biodegradability of indigo dyed wastewaters *J. Hazard. Mater.* **243** 292–301
[19] Kwan C Y, Chu W and Lam W S 2007 The role of oxalate in the kinetics of 2,4-D oxidation over ferrous ion-supported catalysts *J. Mol. Catal. A Chem.* **274** 50–7
[20] Liu L, Chen Z, Zhang J, Shan D, Wu Y, Bai L and Wang B 2021 Treatment of industrial dye wastewater and pharmaceutical residue wastewater by advanced oxidation processes and its combination with nanocatalysts: A review *J. Water Process Eng.* **42** 102122
[21] Lin K Y A and Chen B J 2017 Magnetic carbon-supported cobalt derived from a Prussian blue analogue as a heterogeneous catalyst to activate peroxymonosulfate for efficient degradation of caffeine in water *J. Colloid Interface Sci.* **486** 255–64
[22] Lagos K J, Marinkovic B A, Dosen A, Guamán M V., Guerrero V H, Pardo E and Pontón P I 2020 Data on phase and chemical compositions of black sands from "El Ostional" beach situated in Mompiche, Ecuador *Data Br.* **32** 106214
[23] Valdivieso-Ramírez C S, Pontón P I, Dosen A, Marinkovic B A and Guerrero V H 2022 One-Step Synthesis of Iron and Titanium-Based Compounds Using Black Mineral Sands and Oxalic Acid under Subcritical Water Conditions *Minerals* **12** 306
[24] Liu S, Wang X and Zhang J 2020 Fenton-like reaction and photocatalysis using ferrous oxalate and G-C3 N4 enhancing reactive oxygen species for dye wastewater degradation under visible-light irradiation *Desalin. Water Treat.* **193** 359–68
[25] Frost R L 2004 Raman spectroscopy of natural oxalates *Anal. Chim. Acta* **517** 207–14
[26] Zhang T, Oyama T, Aoshima A, Hidaka H, Zhao J and Serpone N 2001 Photooxidative N-demethylation of methylene blue in aqueous TiO2 dispersions under UV irradiation *J. Photochem. Photobiol. A Chem.* **140** 163–72
[27] Kwan C, Technology W C-W S and and 2004 undefined 2004 Photooxidation of 2, 4-dichlorophenoxyacetic acid by ferrous oxalate-mediated system *iwaponline.com*
[28] Kolayli S, Ocak M, Küçük M and Abbasoğlu R 2004 Does caffeine bind to metal ions? *Food Chem.* **84** 383–8
[29] Nafisi S, Sadjadi A S, Zadeh S S and Damerchelli M 2003 Interaction of metal ions with caffeine and theophylline: Stability and structural features *J. Biomol. Struct. Dyn.* **21** 289–95
[30] Jabbar M A, Kabir M H and Chowdhury R A 2013 Influence Of Caffeine On The Redox Characteristics Of Iron In Aqueous Solution *J. Bangladesh Chem. Soc.* **25** 166–79
[31] Calatayud J M and Zamora L L 2013 Spectrophotometry | Pharmaceutical Applications *Encycl. Anal. Sci.* 249–62
[32] Dalga B and Belay A 2017 Study of the self-association of caffeine and chlorogenic acid and their hetero-association with methylene blue using spectrophotometric method *rjb.ro* **27** 35–53

[33] Dalmázio I, Santos L S, Lopes R P, Eberlin M N and Augusti R 2005 Advanced oxidation of caffeine in water: On-line and real-time monitoring by electrospray ionization mass spectrometry *Environ. Sci. Technol.* **39** 5982–8
[34] Rao Y, Long H and Hao J 2021 The oxidative degradation of Caffeine in UV/Fe(II)/persulfate system—Reaction kinetics and decay pathways *Water Environ. Res.* **93** 559–69
[35] Norazmi N, Rasad Z R A, Mohamad M and Manap H 2017 Uric acid detection using uv-vis spectrometer *IOP Conf. Ser. Mater. Sci. Eng.* **257**
[36] Nuevo M, Milam S N, Sandford S A, Elsila J E and Dworkin J P 2009 Formation of uracil from the ultraviolet photo-irradiation of pyrimidine in pure H2O ices *Astrobiology* **9** 683–95